ResearchGate

See discussions, stats, and author profiles for this publication at: https://www.researchgate.net/publication/51925534

In situ Generation of Well-Dispersed ZnO Quantum Dots on Electrospun Silica Nanotubes with High Photocatalytic Activity

ARTICLE *in* ACS APPLIED MATERIALS & INTERFACES · DECEMBER 2011

Impact Factor: 6.72 · DOI: 10.1021/am201420b · Source: PubMed

CITATIONS
20

READS
35

10 AUTHORS, INCLUDING:

Xin Zhang
Northeast Normal University
17 PUBLICATIONS **249** CITATIONS
SEE PROFILE

Zhenyi Zhang
Dalian Nationalities University
46 PUBLICATIONS **1,936** CITATIONS
SEE PROFILE

Peng Zhang
Northeast Normal University
31 PUBLICATIONS **1,323** CITATIONS
SEE PROFILE

Mingyi Zhang
Harbin Normal University
60 PUBLICATIONS **1,766** CITATIONS
SEE PROFILE

Available from: Xin Zhang
Retrieved on: 01 February 2016

ACS APPLIED MATERIALS & INTERFACES

Research Article

www.acsami.org

In situ Generation of Well-Dispersed ZnO Quantum Dots on Electrospun Silica Nanotubes with High Photocatalytic Activity

Xin Zhang, Changlu Shao,* Zhenyi Zhang, Jinhuan Li,* Peng Zhang, Mingyi Zhang, Jingbo Mu, Zengcai Guo, Pingping Liang, and Yichun Liu

Center for Advanced Optoelectronic Functional Materials Research, and Key Laboratory of UV Light-Emitting Materials and Technology of Ministry of Education, Northeast Normal University, 5268 Renmin Street, Changchun 130024, People's Republic of China

ABSTRACT: The ZnO quantum dots-SiO_2 nanotubes (ZQDs-SNTs) nanocomposite was successfully fabricated by direct heat treatment of the electrospun zinc acetate/tetraethyl orthosilicate (TEOS)/polymer nanotubes (NTs). The results indicated that the ZnO quantum dots (ZQDs) with diameter about 3−5 nm were highly dispersed on the SiO_2 nanotubes (SNTs). And, there might be Zn−O−Si bonds between ZQDs and SiO_2 matrix, which formed interface states in the ZQDs-SNTs nanocomposite. The photocatalytic studies revealed that the ZQDs-SNTs nanocomposite exhibited high photocatalytic activity to degrade Rhodamine B (RB) under ultraviolet (UV) light irradiation, which might be ascribed to two reasons. The first one was the high dispersity of ZQDs; another one was the high separation efficiency of photogenerated electron−hole pairs due to the trap effect for photogenerated electrons of the interface states between ZQDs and SiO_2. During the photocatalytic reaction, the ZQDs-SNTs nanocomposite also exhibited high chemical stability in a wide range of pH values, which might be ascribed to the protective action of SiO_2 and the presence of Zn−O−Si bonds between ZQDs and SiO_2. Furthermore, the ZQDs-SNTs nanocomposites could be easily recycled because of their one-dimensional nanostructure property.

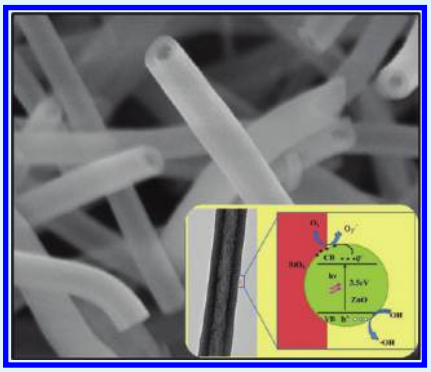

KEYWORDS: *ZnO quantum dots, SiO_2 nanotubes, nanocomposite, electrospinning, photocatalysis, degradation*

1. INTRODUCTION

As a wide-band gap semiconductor (E_g = 3.25−3.5 eV) with an extremely large exciton binding energy of 60 meV, ZnO has many desirable physical properties which have been used in UV lasers, photodetectors, solar cells, gas sensors, field-effect transistors, photocatalysis and so on.[1−11] The potential use in photocatalysis for degradation of environmental pollutants has particularly aroused great interest due to its nontoxic nature and low cost.[2,12] In particular, the nanosized ZnO exhibits high photocatalytic activity due to its high surface-to-volume ratio.[13] As a result, ZnO quantum dots (ZQDs) with smaller size will be an excellent photocatalyst with higher photocatalytic activity. However, as a photocatalyst, ZQDs have two typically disadvantages: (1) ZQDs very easily aggregate to minimize their surface area due to their high surface energy, resulting in lower catalytic activities; (2) ZQDs are impractical for industrial applications because the suspended ZQDs are easily lost in the process of photocatalytic reaction and separation, which may pollute the treated water again. In order to overcome these disadvantages of the ZQDs, increasing researchers have made effort to introduce the nanosized photocatalyst on/into solid supports (such as polymer, carbon, metal oxides, SiO_2 and so on) to form composite catalysts.[14−17] Among the different materials, SiO_2 has been deemed as excellent catalyst support because of their chemical inertia, thermal stability, and high transmissivity to the UV radiation; also, their high absorption might facilitate the interface reaction to organic compounds. It is worth pointing out that nanostructural SiO_2 supports have attracted more and more attention because of the large specific surface areas. Especially, the SiO_2 supports with one-dimensional (1D) nanostructure possess favorable recycling characteristics compared with SiO_2 nanoparticles and high surface area to volume ratio compared with SiO_2 nanofilms, which make them a good candidate for catalytic reaction in practical industry. Especially, the hollow 1D nanostructural SiO_2 (such as hollow SiO_2 nanofibers and SiO_2 nanotubes (SNTs)) will be better catalyst supports due to their higher surface area to volume ratio compared with the solid 1D nanostructural SiO_2. As for how to prepare the hollow 1D nanostructural SiO_2, a rich variety of methods such as template methods, thermal evaporation, electrospinning, and so forth have been exploited.[18−21] Notably, electrospinning is a remarkably simple and effective technique to prepare the hollow 1D nanostructural SiO_2. In our previous study, we proposed a new method to fabricate tetraethyl orthosilicate (TEOS)/polymer nanotubes (NTs) via a single spinneret electrospinning technique in terms of solvent evaporation induced phase separation.[22] And, we obtained the SNTs by direct heat

Received: October 16, 2011
Accepted: December 27, 2011
Published: December 27, 2011

 © 2011 American Chemical Society

treatment of the above NTs because of the residual TEOS in the wall of TEOS/polymer NTs in our subsequent work.[23]

In our present work, we introduced the zinc acetate into the precursor to fabricate the zinc acetate/TEOS/polymer NTs via single spinneret electrospinning technique. By the further heat treatment of the above NTs, the ZQDs-SNTs nanocomposite was obtained, and the photocatalytic activity of the ZQDs-SNTs nanocomposite was investigated by measuring the degradation of dye Rhodamine B (RB) as a test substance. The experimental results showed that the obtained ZQDs-SNTs nanocomposite exhibited high photocatalytic activity, and the high photocatalytic activity could be kept in a wide range of pH values. Furthermore, because of their 1D nanostructure property, the ZQDs-SNTs nanocomposite could be easily recycled. Finally, postulate mechanism for the photocatalysis of the ZQDs-SNTs nanocomposite was proposed.

2. EXPERIMENTAL SECTION

2.1. Materials. Polyvinylpyrrolidone (PVP, M_w = 1 300 000), zinc acetate ($Zn(CH_3COO)_2$ $2H_2O$) and TEOS were purchased from Tianjin Chemicals (Tianjin, China). Ethanol was purchased from Beijing Chemicals (Beijing, China). All materials were directly used as received without further purification.

2.2. Preparation of the ZQDs-SNTs Nanocomposite. First, 1 g of PVP was dissolved in 10 mL of ethanol. When the PVP was dissolved completely, 0.118 g of zinc acetate was added to the PVP solution. After 10 h, 1 mL of TEOS was slowly dropped into the mixed solution to obtain the precursor. Two hours later, the precursor was transferred into a plastic syringe for electrospinning. The positive voltage was 10 kV, and the distance between the needle tip and the collector was about 12−15 cm, resulting in a dense web of the electrospun zinc acetate/TEOS/polymer NTs being collected on the aluminum foil. Afterward, the as-spun NTs were calcined at a rate of 30 °C/h and remained for 2 h at 600 °C to form the ZQDs-SNTs nanocomposite (Scheme 1). For comparison, pure SNTs were prepared by the same route as for the ZQDs-SNTs nanocomposite, except that no zinc acetate was added.

Scheme 1. Schematic Diagram of the Fabrication of the ZQDs-SNTs Nanocomposite

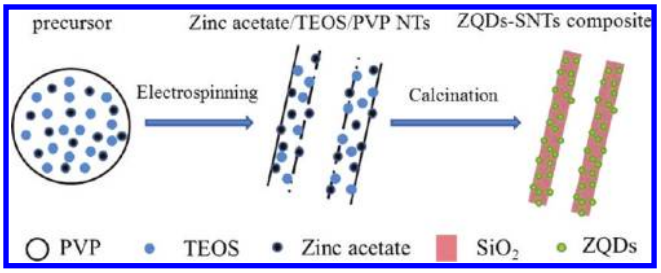

2.3. Characterization. The morphologies of the as-prepared ZQDs-SNTs nanocomposite were observed by a scanning electron microscope (SEM; XL-30 ESEM FEG, Micro FEI Philips) and transmission electron microscopy (TEM; Hitachi 600). Energy dispersive X-ray (EDX) spectroscopy being attached to scanning electron microscopy (SEM) was used to analyze the composition of samples. X-ray diffraction (XRD) measurements were carried out using a D/max 2500 XRD spectrometer (Rigaku) with Cu K line of 0.1541 nm. X-ray photoelectron spectroscopy (XPS) was performed on a VG ESCALAB LKII instrument with Mg KR-ADES ($h\nu$ = 1253.6 eV) source at a residual gas pressure of below 1 × 10^{-8} Pa.

2.4. Photocatalytic Test. The photoreactor was designed with an internal light source surrounded by a water-cooling quartz jacket (50 W high-pressure mercury lamp with main emission wavelength of 313 nm), where 100 mL of the RB solution with an initial concentration of 10 mg/L in the presence of photocatalyst (0.01 g). The solution was stirred in the dark for 30 min to obtain a good dispersion and establish adsorption−desorption equilibrium between the organic molecules and the catalyst surface. Decreases in the concentrations of dyes were analyzed by a Cary 500 UV−vis−-NIR spectrophotometer. At given intervals of illumination, the samples (4 mL) of the reaction solution were taken out and analyzed.

3. RESULTS AND DISCUSSION

3.1. Morphology of the As-Prepared ZQDs-SNTs Nanocomposite. Figure 1a and b showed the SEM images of the as-prepared sample. It could be observed that the diameters of the ZQDs-SNTs nanocomposite were mainly about 280−400 nm with extremely smooth surfaces and long length. Meanwhile, the ruptured sections in images a and b in Figure 1 clearly showed the tubular structure of the nanocomposite. The EDX spectroscopy of the sample displayed in Figure 1c showed that Zn, Si, and O elements existed in the sample. In addition, EDX analysis indicated that the molar ratio of Zn to Si was about 1:4 for ZQDs-SNTs nanocomposite. Figure 1d showed the TEM image of a ruptured nanotube with inner diameter of about 250 nm and wall thickness of about 75 nm. Under higher magnification, the small ZQDs (3−5 nm) were evenly dispersed on the SNTs walls (Figure 1e). A representative high-resolution TEM (HRTEM) image taken from the selected rectangle area of Figure 1e was shown in the Figure 1f. The lattice fringes were clearly visible with a spacing of about 0.246 nm, which corresponded to the lattice spacing of the (101) planes of ZnO. Furthermore, the inset of Figure 1d showed the corresponding selected area electron diffraction (SAED) pattern, which could confirm that the ZQDs with polycrystalline configuration existed in the nanocomposite.

3.2. XRD Patterns of the ZQDs-SNTs Nanocomposite. Figure 2 illustrated the XRD pattern of ZQDs-SNTs nanocomposite. The wide angle XRD patterns showed only the diffraction peak of noncrystalline SiO_2 frameworks, and no characteristic peaks belonging to ZQDs were found in the ZQDs-SNTs nanocomposite. The absence of XRD peaks of ZQDs was ascribed to their very small size (about 3−5 nm), low content and high dispersion in SNTs.[24−26]

3.3. XPS Spectra of the ZQDs-SNTs Nanocomposite. To further investigate the presence of ZQDs in the ZQDs-SNTs nanocomposite and the interaction of ZQDs and SiO_2, we measured the XPS spectra of the sample. The fully scanned spectrum of the ZQDs-SNTs nanocomposite was showed in the Figure 3a. The overview spectra demonstrated that no extra peak corresponding to any impurities other than Si, Zn, O, and C existed in ZQDs-SNTs nanocomposite. In the Figure 3b, The Zn 2p spectrum showed two symmetric peaks, the peak centered at 1022.2 eV corresponded to the Zn $2p_{3/2}$ and another one centered at 1045.0 eV was assigned to Zn $2p_{1/2}$, indicating a normal state of Zn^{2+} in the ZQDs-SNTs nanocomposite. Furthermore, the binding energy of Zn $2p_{3/2}$ in the ZQDs-SNTs nanocomposite was 1022.2 eV, which was 1.1 eV higher than the value of pure ZnO (1021.1 eV).[27−29] Because of the valence electron density of Zn in the Zn−O−Si bond was lower than that in the Zn−O−Zn bond, it was reasonable to ascribe the shift of binding energy of Zn $2p_{3/2}$ to the formation of Zn−O−Si band between ZQDs and SiO_2 matrix.[27−30] As shown in the Figure 3c, the O 1s peak centered at about 532.8 eV was asymmetric, indicating the presence of more than one chemical environment for oxygen species. The

dx.doi.org/10.1021/am201420b | ACS Appl. Mater. Interfaces 2012, 4, 785−790

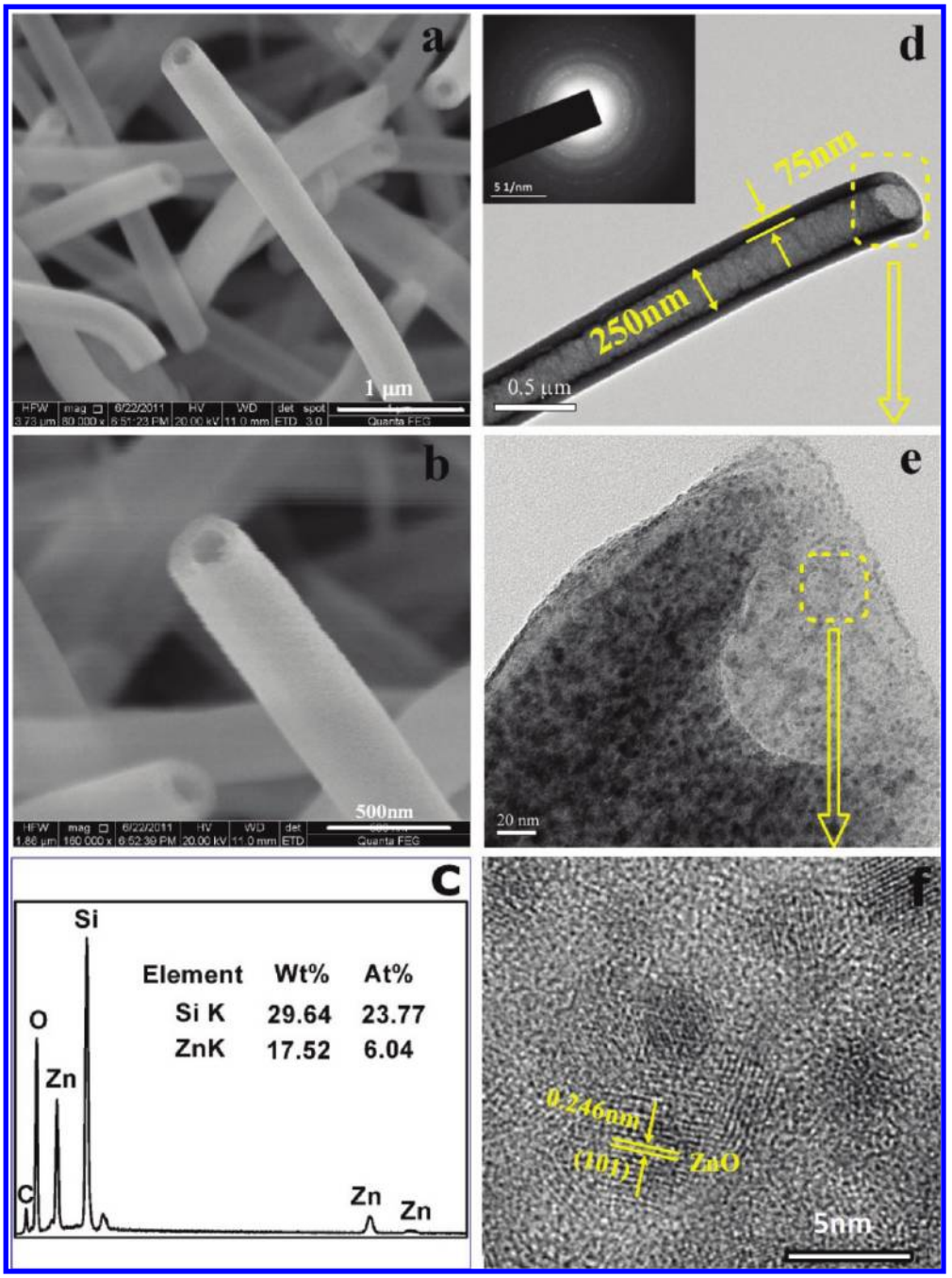

Figure 1. (a, b) SEM image of the ZQDs-SNTs nanocomposite at low magnification and high magnification; (c) EDX spectrum of the ZQDs-SNTs; (d, e) TEM image of the ZQDs-SNTs nanocomposite at low magnification and high magnification; the inset is the corresponding selected area electron diffraction pattern; (f) HRTEM image of the ZQDs-SNTs nanocomposite.

O 1s peak could be fitted with two peaks. The main peak at 532.8 eV could be assigned to the oxygen in the noncrystalline SiO_2.[30] In our work, most of oxygen was captured by noncrystalline SiO_2. The quantitative analysis of the Zn and relative O was completed using the XPS peak area data of Zn 2p and O 1s (peak at 531.2 eV) and their respective elemental sensitivity factor according to the equation (eq) below

$$n(\mathrm{E1})/n(\mathrm{E2}) = [A(\mathrm{E1})/S(\mathrm{E1})]/[A(\mathrm{E2})/S(\mathrm{E2})] \quad (1)$$

where n is the number of the atom, Ei was the element i, A is the peak area, and S is the elemental sensitivity factor.[31] The content ratio of Zn and O was about 1:1.07, indicating that the peak at 531.2 eV could be attributed to the oxygen in ZQDs. Furthermore, the O 1s peak assigned to ZQDs was 0.4 eV higher than that of pure ZnO (530.8 eV), which indicated the formation of Si−O−Zn bond on the surfaces of ZQDs.[32] From the results of XPS spectra, the interaction of the ZQDs surface with SiO_2 was shown through a possible model displayed in Scheme 2. Furthermore, when the photoexcited electron−hole pairs were generated under UV light irradiation, the interface states could act as trap centers for the photogenerated electrons, which might be favorable to enhance the separation efficiency of photogenerated electrons and holes, and then account for the high photocatalytic activity of the ZQDs-SNTs nanocomposite.[33]

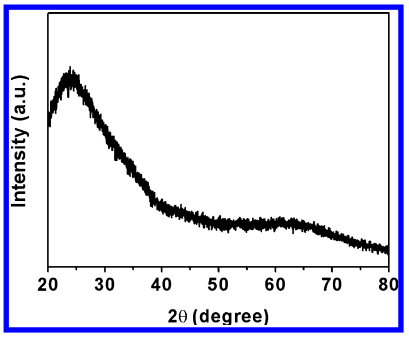

Figure 2. XRD Patterns of the ZQDs-SNTs nanocomposite.

3.4. Photocatalytic Activity of the ZQDs-SNTs Nanocomposite. The photocatalytic activity of the ZQDs-SNTs nanocomposite was evaluated by the degradation of RB in aqueous solution under UV light irradiation. In the experiment, the degradation efficiency of the as-prepared samples was defined as C/C_0, where C and C_0 stood for the remnants and initial concentration of RB, respectively. And, the time from −30 to 0 min in the Figure 4 showed the adsorption−desorption of RB process in the presence of photocatalysts in the dark before photocatalytic degradation profiles of RB with UV light irradiation. As observed in Figure 4a, the control experiments were performed under different conditions: (1) in the presence of photocatalysts but in the dark and (2) with UV light irradiation but in the absence of the photocatalysts. These results illuminated that there was no appreciable degradation of RB after 50 min in the absence of photocatalysts. And, the adsorption−desorption equilibrium of RB in the dark was established within 30 min. Figure 4b showed the degradation curves of RB on the pure SNTs and ZQDs-SNTs nanocomposite. It could be observed that ZQDs-SNTs nanocomposite exhibited high catalytic activity compared with pure SNTs. And the reaction over ZQDs-SNTs nanocomposite was almost complete within 50 min. Furthermore, it was well-known that as an amphoteric oxide, ZnO would be degraded in acidic and alkaline solution resulted in the decrease in photocatalytic activity. To evaluate the photocatalytic activity stability of our sample, we carried out the experiments of the photocatalytic degradation of RB at different pH values (3, 7, and 11). As observed in Figure 4c, the photocatalytic activity almost unchanged at different pH values, which might be attributed to the improved chemical stability caused by the protective action of SiO_2 and the presence of Zn−O−Si bonds between ZQDs and SiO_2. Figure 4d showed the photocatalytic degradation of RB over the ZQDs-SNTs nanocomposite with three times (at pH value of 7). It indicated that this nanocomposite photocatalysts could be easily recycled without a decrease of photocatalytic activity due to their 1D nanostructure property. These properties would broaden its potential application in pollutant treatment.

Scheme 2. Model Showing the Surface Interaction of ZQDs with Long-Chain SiO_2 Molecules

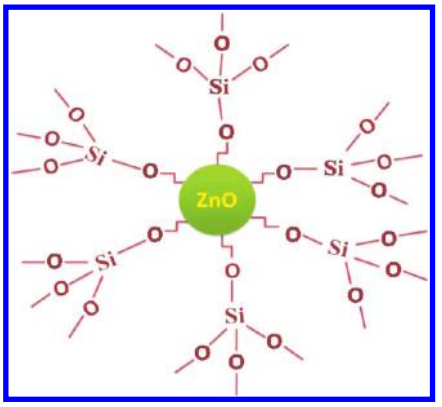

On the basis of the above experimental results and the theory analysis, a proposed mechanism for the photocatalysis of the ZQDs-SNTs nanocomposite was illustrated in Scheme 3. In our work, the ZQDs were highly dispersed in SNTs, leading to the large surface areas of ZQDs and large number of interface states between ZQDs and SiO_2 which were in charge of the high catalytic activity exhibited by ZQDs-SNTs nanocomposite. When the UV illuminated, the photogenerated electrons in the conduction band of ZQDs were trapped at the interface states between ZQDs and SiO_2 while the photogenerated holes were left in the valence band of ZQDs to migrate to the surface, suggesting that the photogenerated electrons and holes were efficiently separated. The effective charge separation could account for the high activity of the ZQDs-SNTs nanocomposite. The major reactions that occur in our study could be described by equations eqs 2−8.

$$\text{ZQDs} - \text{SNTs} + h\nu \rightarrow e^-(\text{interface states}) + h^+(\text{ZQDs}) \quad (2)$$

$$e^- + O_2 \rightarrow O_2 \bullet^- \quad (3)$$

$$O_2 \bullet^- + H_2O \rightarrow HO_2 \bullet + OH^- \quad (4)$$

$$HO_2 \bullet + H_2O \rightarrow H_2O_2 + OH\bullet \quad (5)$$

$$H_2O_2 \rightarrow 2OH \bullet \quad (6)$$

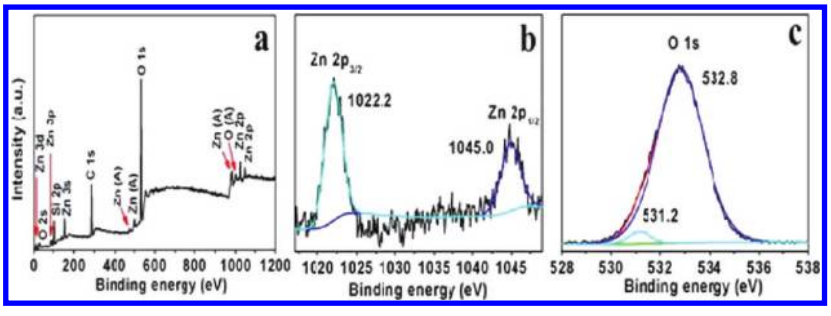

Figure 3. (a) XPS fully scanned spectra of the ZQDs-SNTs nanocomposite; (b) Zn 2p and (c) O 1s. ("Zn (A)" and "O (A)" in a are Auger peaks of Zn and O).

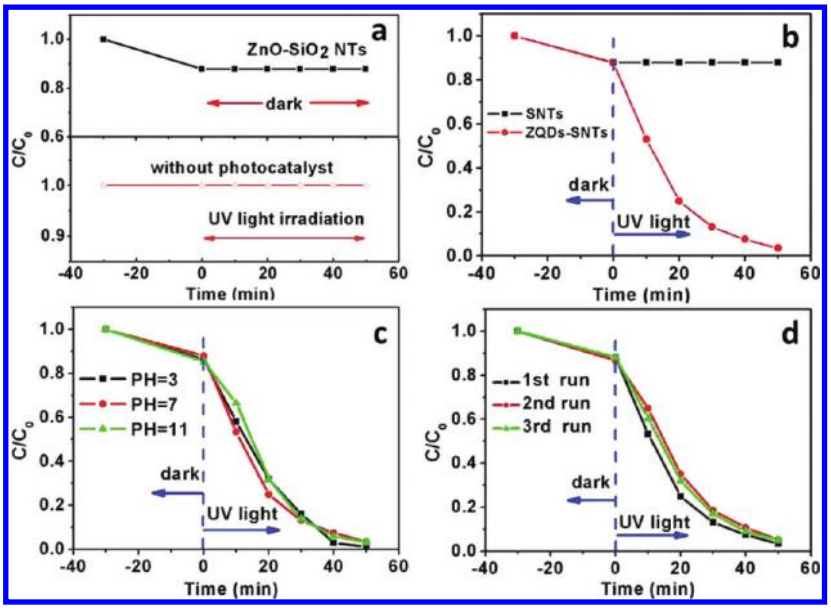

Figure 4. (a) Degradation profiles of RB in the presence of the photocatalysts but in the dark and with UV light irradiation but in the absence of the photocatalysts; (b) degradation profiles of RB over the sample: pure SNTs and ZQDs-SNTs nanocomposite; (c) degradation profiles of RB at three different pH values (3, 7, 11) over ZQDs-SNTs nanocomposite; (d) Photocatalytic activity of the ZQDs-SNTs nanocomposite for RB degradation with three times of cycling uses (pH = 7).

Scheme 3. Postulate Mechanism for the Photocatalysis of the ZQDs-SNTs Nanocomposite

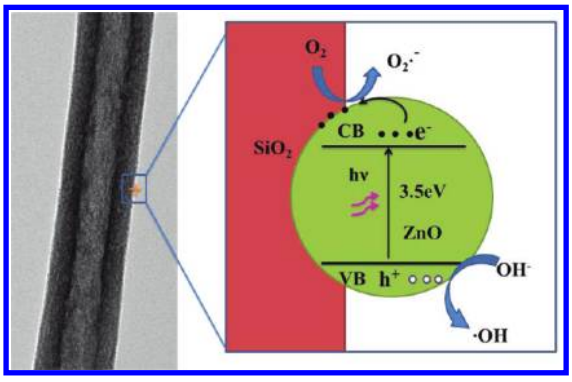

$$h^+ + OH^- \rightarrow OH\bullet \quad (7)$$

$$OH\bullet + RB \rightarrow CO_2 + H_2O \quad (8)$$

Under UV light irradiation, the photogenerated electron–hole pairs were generated (eq 2). Subsequently, the photogenerated electrons in conduction band of ZQDs transferred to the interface states between ZQDs and SiO_2; meanwhile, the excess of valence band holes were left in the ZQDs. Dissolved oxygen molecules (O_2) reacted with interface trap centers electrons (e^-) to yield superoxide radical anions ($O_2\bullet^-$) (eq 3), which on protonation generated the hydroperoxy radicals ($HO_2\bullet$) (eq 4), producing hydroxyl radicals ($OH\bullet$) (eqs 5 and 6). The holes (h^+) were trapped by surface hydroxyl groups (or H_2O) at the catalyst surface to yield $OH\bullet$ (eq 7), which was a strong oxidizing agent to decompose the organic dye (eq 8).[34,35]

4. CONCLUSIONS

In summary, the ZQDs-SNTs nanocomposite was fabricated by direct heat treatment of the electrospun zinc acetate/TEOS/polymer NTs. The investigation of photocatalytic ability indicated that the ZQDs-SNTs nanocomposite possessed high photocatalytic activity and high chemical stability in a wide range of pH values. Furthermore, the ZQDs-SNTs nanocomposite could be easily recycled without decrease of the photocatalytic activity due to its 1D nanostructure property and high chemical stability. Also, it is expected that the ZQDs-SNTs nanocomposite with high photocatalytic activity and high chemical stability will greatly promote their practical application to eliminate the organic pollutants from wastewater.

AUTHOR INFORMATION

Corresponding Author

*E-mail: clshao@nenu.edu.cn (C.S.); lijh248@nenu.edu.cn (J.L.). Tel. 8643185098803.

ACKNOWLEDGMENTS

The present work is supported financially by the National Natural Science Foundation of China (50572014, 50972027), the Program for New Century Excellent Talents in University (NCET-05-0322), and the Fundamental Research Funds for the Central Universities (11SSXT005).

REFERENCES

(1) Peng, Y.; Hsieh, T.; Hsu, C. *Nanotechnology* **2006**, *17*, 174–180.
(2) McLaren, A.; Valdes-Solis, T.; Li, G.; Tsang, S. C. *J. Am. Chem. Soc.* **2009**, *131*, 12540–12541.
(3) Bera, A.; Basak, D. *ACS Appl. Mater. Interfaces* **2009**, *1*, 2066–2070.
(4) Huang, M. H. *Science* **2001**, *292*, 1897–1899.
(5) Kind, H.; Yan, H.; Messer, B.; Law, M.; Yang, P. *Adv. Mater.* **2002**, *14*, 158–160.
(6) Law, M.; Greene, L. E.; Johnson, J. C.; Saykally, R.; Yang, P. *Nat. Mater.* **2005**, *4*, 455–459.
(7) Zhang, Z.; Li, X.; Wang, C.; Wei, L.; Liu, Y.; Shao, C. *J. Phys. Chem. C* **2009**, *113*, 19397–19403.
(8) Goldberger, J.; Sirbuly, D. J.; Law, M.; Yang, P. *J. Phys. Chem. B* **2004**, *109*, 9–14.

(9) Zheng, Y.; Chen, C.; Zhan, Y.; Lin, X.; Zheng, Q.; Wei, K.; Zhu, J.; Zhu, Y. *Inorg. Chem.* **2007**, *46*, 6675−6682.
(10) Li, G. R.; Hu, T.; Pan, G. L.; Yan, T. Y.; Gao, X. P.; Zhu, H. Y. *J. Phys. Chem. C* **2008**, *112*, 11859−11864.
(11) Wang, J.; Liu, P.; Fu, X.; Li, Z.; Han, W.; Wang, X. *Langmuir* **2009**, *25*, 1218−1223.
(12) Akyol, A.; Yatmaz, H. C.; Bayramoglu, M. *Appl. Catal., B* **2004**, *54*, 19−24.
(13) Bohle, D. S.; Spina, C. J. *J. Am. Chem. Soc.* **2009**, *131*, 4397−4404.
(14) Hong, R.; Li, J.; Chen, L.; Liu, D.; Li, H.; Zheng, Y.; Ding, J. *Powder Technol.* **2009**, *189*, 426−432.
(15) Mu, J.; Shao, C.; Guo, Z.; Zhang, Z.; Zhang, M.; Zhang, P.; Chen, B.; Liu, Y. *ACS Appl. Mater. Interfaces* **2011**, *3*, 590−596.
(16) Zhu, H.; Xiao, L.; Jiang, R.; Zeng, G.; Liu, L. *Chem. Eng. J.* **2011**, *172*, 746−753.
(17) Panigrahi, S.; Bera, A.; Basak, D. *J. Colloid Interface Sci.* **2011**, *353*, 30−38.
(18) Fan, X.; Meng, X.-M.; Zhang, X.-H.; Lee, C.-S.; Lee, S.-T. *Appl. Phys. Lett.* **2007**, *90*, 103114.
(19) Zhai, T.; Gu, Z.; Dong, Y.; Zhong, H.; Ma, Y.; Fu, H.; Li, Y.; Yao, J. *J. Phys. Chem. C* **2007**, *111*, 11604−11611.
(20) Liu, L. Z.; Wu, X. L.; Zhang, Z. Y.; Xu, L. L.; Li, T. H.; Chu, P. K. *J. Nanosci. Nanotechnol.* **2010**, *10*, 5583−5586.
(21) Zhan, S.; Chen, D.; Jiao, X. *J. Colloid Interface Sci.* **2008**, *318*, 331−336.
(22) Li, X. H.; Shao, C. L.; Liu, Y. C. *Langmuir* **2007**, *23*, 10920−10923.
(23) Zhang, Z.; Shao, C.; Zou, P.; Zhang, P.; Zhang, M.; Mu, J.; Guo, Z.; Li, X.; Wang, C.; Liu, Y. *Chem. Commun.* **2011**, *47*, 3906.
(24) Zhang, Z.; Shao, C.; Gao, F.; Li, X.; Liu, Y. *J. Colloid Interface Sci.* **2010**, *347*, 215−220.
(25) Zhang, P.; Shao, C.; Zhang, Z.; Zhang, M.; Mu, J.; Guo, Z.; Sun, Y.; Liu, Y. *J. Mater. Chem.* **2011**, *21*, 17746.
(26) Wang, N.; Zhou, T.; Wang, J.; Yuan, H.; Xiao, D. *Analyst* **2010**, *135*, 2386.
(27) Fu, Z.; Yang, B.; Li, L.; Dong, W.; Jia, C.; Wu, W. *J. Phys.: Condens. Matter* **2003**, *15*, 2867.
(28) Jiang, Q.; Wu, Z. Y.; Wang, Y. M.; Cao, Y.; Zhou, C. F.; Zhu, J. H. *J. Mater. Chem.* **2006**, *16*, 1536−1542.
(29) Yao, B.; et al. *J. Phys.: Condens. Matter.* **2000**, *12*, 6265.
(30) Lu, Q.; Wang, Z.; Li, J.; Wang, P.; Ye, X. *Nanoscale Res. Lett.* **2009**, *4*, 646−654.
(31) Li, J. H.; Shen, D. Z.; Zhang, J. Y.; Zhao, D. X.; Li, B. S.; Lu, Y. M.; Liu, Y. C.; Fan, X. W. *J. Magn. Magn. Mater.* **2006**, *302*, 118.
(32) Peng, W. Q.; Qu, S, C.; Cong, , G. W.; Wang, Z. G. *Cryst. Growth Des.* **2006**, *6*, 1518−1522.
(33) Panigrahi, S.; Bera, A.; Basak, D. *ACS Appl. Mater. Interfaces* **2009**, *1*, 2408−2411.
(34) Aarthi, T.; Madras, G. *Ind. Eng. Chem. Res.* **2007**, *46*, 7−14.
(35) Rajeshwar, K.; Osugi, M.; Chanmanee, W.; Chenthamarakshan, C.; Zanoni, M.; Kajitvichyanukul, P.; Krishnan, A. R. *J. Photochem.Photobiol., C* **2008**, *9*, 171−192.